Single Point Positioning with Vertical Total Electron Content estimation based on single epoch data

Artur Fischer[1], Sławomir Cellmer[1], and Krzysztof Nowel[1]

[1]Department of Geodesy, University of Warmia and Mazury, Olsztyn, 10-719, Poland

Correspondence to: Artur Fischer (artur.fischer21@gmail.com)

Abstract. This paper proposes a new mathematical method of ionospheric delay estimation in single point positioning (SPP) using a single-frequency receiver. The proposed approach focuses on the *ΔVTEC* component estimation (MSPPwithdVTEC) with the assumption of an initial and constant value equal to 5 in any observed epoch. The principal purpose of the study is to examine the reliability of this approach to become independent from the external data in the ionospheric correction calculation process. To verify the MSPPwithdVTEC, the SPP with the Klobuchar algorithm was employed as a reference model, utilizing the coefficients from the navigation message. Moreover, to specify the level of precision of the MSPPwithdVTEC, the SPP with the IGS TEC map was adopted for comparison as the high-quality product in the ionospheric delay determination. To perform the computational tests, real code data was involved from three different localizations in Scandinavia using two parallel days. The criterion were the ionospheric changes depending on geodetic latitude. Referring to the Klobuchar model, the MSPPwithdVTEC obtained a significant improvement of 15 – 25% in the final SPP solutions. For the SPP approach employing the IGS TEC map and for the MSPPwithdVTEC, the difference in error reduction was not significant, and it did not exceed 1.0% for the IGS TEC map. Therefore, the MSPPwithdVTEC can be assessed as an accurate SPP method based on error reduction value, close to the SPP approach with the IGS TEC map. The main advantage of the proposed approach is that it does not need external data.

1 Introduction

Single point positioning (SPP) allows of the indication of an autonomous position of a receiver using code data from different Global Navigation Satellite Systems (GNSS). Code ranges are not ambiguous and do not require to apply the precise method of ambiguity initialization (Bakuła, 2020). The principal problem of SPP stems from different types of errors degrading the GPS signal between a rover and a specified satellite in a given epoch. Ionospheric delay contributes to the general GPS error budget by its volatility in the range of 40 – 60 m during daytime and 6 – 12 m at night (US Army Corps of Engineers, 2003).

The ionosphere consists of charged particles that appear because of the ionization process (El-Rabbany, 2002; Awange, 2012). Problems with ionosphere modeling come from difficulties between solar activity and the geomagnetic field interactions (Xu and Xu, 2016). The basic concepts of the GPS signals delay were briefly considered by Golubkov et al. and

30   Kuverova et al. (Golubkov et al., 2018; Kuverova et al., 2018; Golubkov et al., 2019). To specify a suitable magnitude of

31   delayed GPS signal along an appropriate path between satellite and receiver, a proportional quantity such as Total Electron

32   Content (TEC) has to be involved and defined as the linear integral of the density of the particles alongside the ray path

33   (Cooper et al., 2019). The TEC unit is equal to 10^{16} electrons per square meter (in the cross-section of 1 m^2) (Ciraolo, 2005).

34   To calculate and reduce such effect on the GPS code measurement, Stępniak (2016) distinguished different types of models

35   and mathematical estimating methods: physical - theoretical (e.g. Chapman's model), physical - empirical (e.g. IRI and the

36   NeQuick model), mathematical - deterministic (based on a mathematics function), and mathematical – stochastic (based on a

37   large set of processed data used to describe the spatial-temporal changes of ionosphere) e.g. the IGS model.

38   The authors propose the autonomous SPP approach with $\Delta VTEC$ component estimation using single-frequency GPS

39   code observations to be independent of external products, e.g. an IGS TEC map. The disadvantage of the mathematical

40   models is performing an ionospheric effect calculation mostly in post-processing. Since many mathematical approaches to

41   self-sufficient ionospheric delay modeling have been proposed, especially in the carrier phase domain using multi-frequency

42   observations, the authors wanted to introduce a new estimation method employing single-frequency GPS code observations.

43   For instance, Georgiadiou (1994) proposed a mathematical method based on differences between the pseudo-ranges

44   measured on the L1 and L2 carries frequency, respectively (dual-frequency method). The computational tests with

45   comparison to the reference method without ionospheric corrections were done by Camargo et al. (2000), focusing

46   particularly on the pseudo-ranges filtered by the carrier phase. The method of slant delay estimation (STEC – alongside a

47   line of sight) in the L1 carrier reduced 80% of errors related to ionospheric effects in the point positioning technique, also

48   delivering improvement solutions during the ionosphere maximum. Bosy (2005) described a geometry-free linear

49   combination which can be employed to ionosphere modeling, with simultaneous consideration and repair of cycle-slip

50   effects and other parameters of GPS vector - ambiguity and tropospheric effects. Krypiak-Gregorczyk and Wielgosz (2018)

51   proposed the use of multi-frequency GNSS signals for TEC modeling, utilizing the carrier phase bias of a geometry-free

52   linear combination. The received bias accuracy results on the level of 7 – 8 cm allow TEC computation with desirable

53   uncertainty, i.e. lower than 1 TECU. Additionally, an ionosphere-free linear combination as an independent positioning

54   approach can also be well adapted to minimize the ionosphere negative impact on GPS positioning (Teunissen and

55   Kleusberg, 1998). However, Hofmann-Wellenhof et al. (2008) stated that "ionosphere-free" is not an entirely correct name,

56   caused by the approximation existing in the process of making the refractive index. Those authors studied an ionosphere-free

57   approach in the code SPP and achieved a beneficial magnitude of error reduction (50-60%) in relation to the reference SPP

58   model without ionospheric corrections.

59   On the contrary, empirical models do not significantly reduce the ionosphere influence in the GPS positioning as

60   mathematical (deterministic) methods, but can make real-time improvements by using the external data, e.g. coefficients

61   transmitted in the navigation message to correct the signal pseudo-ranges. One of these is the Klobuchar algorithm (see

62   Klobuchar, 1987), which compensates for 50 – 60% of the ionospheric range error, utilizing a single-layer model of the

63   ionosphere (Leick et al., 2015). In the current study, the authors wanted to treat the SPP method with the Klobuchar

algorithm as a reference method, because of its popularity and utility in GPS measurement. A significant improvement can be noted in the vertical component which is the most affected by the atmospheric delay. Júnior et al. (2019) investigated the analysis of the Klobuchar model in the ionospheric delay reduction procedure utilizing code observation in point positioning. The algorithm works clearly when ionosphere activity is significant and improves vertical solutions by 67%. For the horizontal components, the improvement using the Klobuchar algorithm is up to 9% regarding the non-iono model. It should be noted that GPS point positioning using the Klobuchar algorithm can degrade the position because of the constant value of the ionospheric delay (up to 5 ns SET) during nighttime.

High-quality representation of the ionosphere influence on positioning can be obtained by the Global Ionospheric Models (GIMs), used mostly in the post-processing purposes as explained in Ciećko and Grunwald (2020). It is worth noting that Abdelazeem et al. (2016) developed the regional ionospheric model over the European area and implemented it in Precise Point Positioning (PPP), operating in real-time using the real-time service products (RTS) of the International GNSS Service (IGS). The results present an improvement in the accuracy on the level of 40 % (under the mid-latitude region) in the 3D position relating to the IGS-GIM. The accuracy is higher primarily because of the better temporal and spatial resolution of the model (15' and 1° x 1°), while the IGS TEC map includes nodes containing the appropriate VTEC value with a time resolution of 1 hour and a spatial resolution of 2.5° x 5°, respectively for latitude and longitude. In turn, Krypiak-Gregorczyk et al. (2017) prepared the ionosphere model covering the Europe region as well, based on multi-GNSS data. The solutions are beneficial because they have 2-3 times lower RMS value than the results of GIMs, e.g. from IGS. Zhang et al. (2019) also examined global ionospheric maps operating in real-time, dedicated to single-frequency positioning. Chen and Gao (2005) tested the IGS TEC map as the basic condition to assess the precision of the PPP model using different procedures to resolve the ionospheric delay problem such as single-frequency ionosphere-free linear combination (averages un-differenced code and carrier-phase observations on the same frequency) or estimation of the ionospheric effect as an unknown parameter. The advantage of the methods is no need for external products. For instance, the estimation method achieved comparable accuracy in the mid-latitude stations but for the higher latitude, the GIM is still quite better, inversely on the equatorial stations. This encourages a focus on the IGS TEC map as the high accuracy product to authenticate solutions from the suggested approach to SPP, and to validate the autonomous method of the ionospheric delay calculation. It should be noted that although the efficiency of GIMs is not significant using GPS code observations, the accuracy is suitable enough for navigation goals and further development of this concept.

In sum, the motivation of this paper is to analyze a new mathematical method of ionospheric delay estimation to improve the SPP. The authors put forward the hypothesis to be independent of external data use in the meaning of the new method in the ionospheric delay calculation procedure.

2 SPP mathematical models

In this section, the grounds of the common used SPP mathematical models using Klobuchar algorithm and IGS TEC map will be introduced, and the proposition of the new strategy of SPP determination by use of simple as well as

autonomous method to estimate the ionospheric delay. This is followed by the appropriate algorithm presentations with suitable explanations. In addition, the accuracy analysis criteria will be described in view of models credibility procedure.

2.1 SPP with ionospheric corrections using Klobuchar algorithm and IGS TEC map

In this study, the Klobuchar model was adapted as a reference in the SPP accuracy tests. Eight model coefficients transmitted via navigation message are the primary components involved in the algorithm to reduce the ionosphere effect in the SPP. The geodetic coordinates of the GPS antenna, GPS observing time (in seconds) as well as azimuth and elevation of observed satellites as viewed from the receiver are needed to be known. The formula to calculate the ionospheric correction based on the Klobuchar algorithm is as follows (Hofmann-Wellenhof et al., 2008):

$$\Delta T_V^{Iono} = A_1 + A_2 \cos\left(\frac{2\pi(t - A_3)}{A_4}\right) \tag{1}$$

where A_1 is a constant value of 5 ns. In turn, A_2 is a sum of multiplying four α coefficients and the geomagnetic latitude of an ionospheric pierce point φ_{IP}^m. t means GPS time of the ionospheric pierce point. A_3 is 14:00 local time which specifies the highest ionospheric disturbance. A_4 means the same as A_3 but there are four β coefficients are multiplied by φ_{IP}^m.

To obtain an ionospheric delay alongside the GPS signal travel path, the mapping function should be employed. Thus, the concept of the ionospheric point has to be expanded as a piercing point of the GPS wave path and the ionospheric single layer on the specified altitude. Thus, the satellite zenith angle at the piercing point - z' should first be indicated (Hofmann-Wellenhof et al., 2008):

$$\sin z' = \frac{R_e}{R_e + h_m} \sin z_0 \tag{2}$$

R_e is Earth radius 6370 km and z_0 means a zenith angle from the observing site. h_m is defined as the height of the ionospheric pierce point. In general, h_m is identified by the single-layer model where all free electrons are concentrated in the infinitesimal spherical shell at the assumed altitude - 450 km. Other formulations are possible too, for instance, from the Klobuchar algorithm, presented in Rui et al. (2011):

$$mF = 1 + 16 \cdot \left(0.53 - \frac{E}{\pi}\right)^3 \tag{3}$$

where E means an elevation angle in the slant factor calculation.

It should be also noted that the type of mapping function in the atmospheric effect calculation process contributes to the final solution accuracy as well. Allain et al. (2009) examined the tomographic mapping function known as Multi-Instrument Data Analysis System (MIDAS) to ionospheric effect determination for the single-frequency data. Research has shown that daily positioning errors are up to 50% lower in comparison to positioning using the Klobuchar algorithm or International

Reference Ionosphere (IRI) when the surrounding distribution of receivers is favorable. Regardless of the map type, dual-frequency observations allow for even greater precision of the ionospheric effect mitigation in the GPS pseudo-range measurement.

Therefore, the mapping function can be used as an inverse of the cosine function (Hofmann-Wellenhof et al., 2008):

$$\Delta T_s^{Iono} = \Delta T_v^{Iono} / \cos z' \tag{4}$$

Finally, the ionospheric delay alongside the rover-satellite is achieved in seconds. To obtain the metric magnitude of the calculated effect, ΔT_s^{Iono} is multiplied by the speed of light. The Klobuchar algorithm was fully described by Xu (2007). To future elaboration, ΔT_s^{Iono} will be denoted as δ_K where subscript is appropriate for the Klobuchar method.

The second approach is SPP with ionospheric corrections computed based on the IGS TEC map. This method is used to examine and verify the quality of the new autonomous, estimation method of the ionospheric effect in the SPP. Consequently, ionospheric delay as the base formula in the zenith direction can be introduced (Schüler, 2001):

$$\delta_{IT} = \int_{h_m}^{\infty} \frac{C_2}{f^2} = \frac{C}{f^2} \int_{h_m}^{\infty} N_e(h) \cdot dh = \frac{C}{f^2} \cdot VTEC \tag{5}$$

where the subscript is proper for the IGS TEC map product. C is a constant value of 40.3 m^3/s^2, f is an appropriate frequency, and $VTEC$ is naturally the vertical total electron content in TECU units. N_e is electron density factor [electrons/m^3], and h is equal to the travelled ray path from the satellite to the rover. In turn, h_m is the height of the single layer of the ionosphere or height of the piercing point for which the appropriate VTEC value from IGS TEC is interpolating. Hence, there is a need to indicate the geodetic coordinates for ionospheric pierce point using e.g. geometric method formulation (Prol et al., 2017).

Taking into account ionospheric delay as a proportional value to TEC and proportional to the distance covered across the band, the relation of VTEC and TEC can be defined (Leick et al., 2015):

$$VTEC = \cos z' \cdot TEC \tag{6}$$

To integrate VTEC to STEC, the ionospheric mapping function, mentioned in the eq. (2) is presented as an inverse of the cosines function. Note, the original sign z_k' was replaced by z_O' (Leick et al., 2015):

$$F(z_O) = \frac{1}{\cos z'} = \left[1 - \left(\frac{R_e \sin z_O'}{R_e + h_m} \right)^2 \right]^{-\frac{1}{2}} \tag{7}$$

where the adopted z' angle is equivalent to the zenith angle at the piercing point in (4).

Using eq. (5), (6), and (7), the ionospheric correction can be obtained in the ray path direction between satellite-rover:

149 $$\delta_{IT} = \frac{40.3}{f^2} \cdot F(z_O) \cdot VTEC \tag{8}$$

150   Therefore, to briefly explain the mathematical model of SPP with utilized ionospheric corrections, the code observation
151 equation was adapted based on Strang and Borre (2008) with complementary changes:

152 $$\begin{cases} P_r^s = \rho_r^s + c(\Delta t_r - \Delta t^s) + \delta_{TROP} + \delta_K + \varepsilon_P \\ P_r^s = \rho_r^s + c(\Delta t_r - \Delta t^s) + \delta_{TROP} + \delta_{IT} + \varepsilon_P \end{cases} \tag{9}$$

153 where the first equation is concerning on the SPP approach with Klobuchar algorithm and the second one is referring
154 to the IGS TEC map. The left side is the measured pseudo-range P_r^s between receiver r and satellite s. On the right side are
155 the model and estimated magnitudes: the geometrical distance ρ_r^s between receiver r and satellite s (position of the reference
156 station antenna used as a priori coordinates of receiver and satellite coordinates computed by utilization of the ephemeris
157 information), speed of light c, receiver and satellite clock biases: Δt_r, Δt^s, δ_{TROP} tropospheric delay, δ_K ionospheric delay
158 computed using Klobuchar algorithm (eight coefficients from navigation message) or δ_{IT} - based on IGS TEC map utilizing
159 IONEX file and pseudo-range remaining error ε_P, respectively. In the research, the tropospheric corrections were obtained
160 based on Hopfield (see Hopfield, 1969) using model values of the dry and the wet subcomponents. Additionally, the clock
161 bias of satellites has been received by the utilization of satellites' ephemeris data and the relativistic improvements.

2.2 Modified SPP with autonomous VTEC estimation method

163   The essence of the proposed modified SPP method lies in an estimation of the $\Delta VTEC$ term which is a variable
164 component of the ionospheric delay:

165 $$\delta_{IONest} = \frac{40.3 \cdot 10^{16}}{f^2} \cdot F(z_O) \cdot (VTEC_0 + \Delta VTEC) \tag{10}$$

166   The modified SPP model with an independent method of the ionospheric effect estimation in the system of equations:

167 $$\begin{cases} P_1 = \rho_r^{s_1} + c(\Delta t_r - \Delta t^{s_1}) + \delta_{TROP_1} + \delta_{IONest_1} + \varepsilon_1 \\ P_2 = \rho_r^{s_2} + c(\Delta t_r - \Delta t^{s_2}) + \delta_{TROP_2} + \delta_{IONest_2} + \varepsilon_2 \\ . \\ . \\ . \\ P_n = \rho_r^{s_n} + c(\Delta t_r - \Delta t^{s_n}) + \delta_{TROP_n} + \delta_{IONest_n} + \varepsilon_n \\ VTEC^{pseudoobs} = VTEC_0 + \Delta VTEC + \varepsilon_{\Delta VTEC} \end{cases} \tag{11}$$

168 The last row is a pseudo-observation equation in which $VTEC_0$ is the constant, initial value of VTECs in a given epoch,

169 appropriate for all satellite elevation, $\Delta VTEC$ is an estimated ingredient and $\varepsilon_{\Delta VTEC}$ is a remaining error of determining factor. It

170 was decided, after performing many tests, to include this pseudo-observation equation into the SPP approach to ensure a

171 stable GPS solution. The model without the pseudo-observation formula would be too weak to give stable results (note that

172 single epoch positioning is used).

173 After many computational tests, it was assumed that the initial value of $VTEC_0$ in any measured epochs during daytime

174 and nighttime of SPP is **5 TECU.** Therefore, the method does not need external information about VTEC referring to the

175 piercing point on the line of sight receiver – satellite, even if the IGS TEC map is available, it indicates that the model is

176 simple to build and implement into a complex algorithm. The reliability and usefulness will be submitted during the

177 presentation of the results.

178 It is assumed in this method that the "observed" and approximate values are equal:

179 $$VTEC^{pseudoobs} = VTEC_0 \tag{12}$$

180 Continuing, to simplify successive descriptions of the modified SPP approach, the mapping coefficient is denoted:

181 $$mapcoeff = \frac{40.3 \cdot 10^{16}}{f^2} F(z_O) \tag{13}$$

182 The system of code equations (11) after linearization can be introduced in the matrix notation with covariance matrix:

183 $$\mathbf{e} = \mathbf{Ax} - \mathbf{y}, \ \mathbf{C_x} = m_0^2 \mathbf{W^{-1}} \tag{14}$$

184 where:

185 $$\mathbf{e} = \begin{bmatrix} -\varepsilon_1 \\ \vdots \\ -\varepsilon_n \end{bmatrix} \tag{15}$$

186 is a residual vector of theoretical corrections,

187 $$\mathbf{A} = \begin{bmatrix} a_{11} & a_{12} & a_{13} & 1 & mapcoeff^1 \\ \vdots & \vdots & \vdots & \vdots & \vdots \\ a_{n1} & a_{n2} & a_{n3} & 1 & mapcoeff^n \\ \hdashline 0 & 0 & 0 & 0 & 1 \end{bmatrix} \tag{16}$$

188 is a design matrix. The first three columns in first block contains derivatives values from Taylor's series, based on satellite

189 coordinates in the specified epochs (i), approximate rover coordinates (r_o) and geometrical distance between rover and

190 satellite: $a_{i1} = -\dfrac{X^i - X_{r_o}}{\rho_{r_o}^i}, a_{i2} = -\dfrac{Y^i - Y_{r_o}}{\rho_{r_o}^i}, a_{i3} = -\dfrac{Z^i - Z_{r_o}}{\rho_{r_o}^i}$, respectively. The last column in the first block relates to the clock error in

191 meters.

192   The vector of unknowns receives an additional parameter in the adjustment process:

193      $$\mathbf{x} = \begin{bmatrix} \Delta X_r \\ \Delta Y_r \\ \Delta Z_r \\ c\Delta t_r \\ \hline \Delta VTEC \end{bmatrix}$$ (17)

194   The disclosure vector is:

195      $$\mathbf{y} = \begin{bmatrix} y_r^1 \\ \vdots \\ y_r^n \\ \hline 0 \end{bmatrix}$$ (18)

196   where $y_r^i = P_i - \rho_i^r + c\Delta t^i - \delta_{TROP_i} - mapcoeff \cdot VTEC_0$. The last entry amounts to zero because of assumption (12).

197   The weight matrix has been prepared based on pseudo-range measurement error which was assumed as a 2.00 m and

198   appropriate satellite elevation angle. The criterion of the minimal mask was implemented as a 10 degree. After

199   computational tests with theoretical analysis, the weight of the estimated component $\Delta VTEC$ was assumed in the model as 1.

200      $$\mathbf{W} = \left[\begin{array}{ccc|c} \dfrac{1}{\delta^2}\sin(elev_1) & \cdots & 0 & 0 \\ \vdots & \ddots & \vdots & \vdots \\ 0 & \cdots & \dfrac{1}{\delta^2}\sin(elev_n) & 0 \\ \hline 0 & \cdots & 0 & 1 \end{array} \right]$$ (19)

201   The least-squares estimate of the equation (14) is computed from the normal equations together with its covariance

202   matrix with the variance factor: $m_0^2 = \dfrac{\mathbf{e}^T\mathbf{We}}{n-m}$. The number of parameters $m = 5$. Thus, the minimal number of observations

203   should be $n = 6$ to ensure necessary redundancy.

204   **2.3 Accuracy analysis criteria**

205   The basic statistical operator in the experiment is a distance of the solution from the true position *dist* where subscript

206   "*r*" means calculated rover's coordinates and "*t*" regarding to the actual position. Moreover, its average value (*DIST*),

207   computed from solutions obtained from the single epochs with its mean error. The actual position means constant station

208   coordinates provided by the agency, which manage the Continuously Operating Reference Station (CORS) used in the

209   experiment for evaluation of the positioning model accuracy. The formula can be introduced in each epoch in the form of

210   Euclidean distance:

211 $$dist_{ep_i} = \sqrt{(X_r - X_t)^2 + (Y_r - Y_t)^2 + (Z_r - Z_t)^2}$$ (20)

212   The formula to calculate the mean error of average solution is as follows:

213 $$m^2_{dist_{ep_i}} = \mathbf{G}\mathbf{C}_{\hat{\mathbf{X}}_{ep1}}\mathbf{G'}$$ (21)

214 where $\mathbf{C}_{\hat{\mathbf{X}}}$ is a covariance matrix of the parameter vector and $\mathbf{G}$ is a gradient:

215 $$\mathbf{G} = \left[\frac{\Delta X_{ep_i}}{dist_{ep_i}} \quad \frac{\Delta Y_{ep_i}}{dist_{ep_i}} \quad \frac{\Delta Z_{ep_i}}{dist_{ep_i}} \right]$$ (22)

216 where $\Delta X_{ep_i}, \Delta Y_{ep_i}, \Delta Z_{ep_i}$ are the coordinates differences between calculated rover position (r) and the appropriate actual

217 position of reference station (t), $dist_{ep_i}$ are explained in formula (20). The average value is as follows:

218 $$m^2_{DIST} = \frac{1}{n^2}\sum_{i=1}^{n} m^2_{dist_{ep_i}}$$ (23)

219   The NEU (North East Up) coordinates system was used in the comparative analysis, where the calculated rover's

220 position is compared to the actual position. Therefore, the rotation matrix was used to convert the covariance matrix (14) of

221 the parameters to the NEU system:

222 $$\mathbf{C_{NEU}} = \mathbf{R}\mathbf{C}_{\hat{\mathbf{X}}}\mathbf{R}^T$$ (24)

223 where:

224 $$\mathbf{R} = \begin{bmatrix} -\sin\varphi\cos\lambda & -\sin\varphi\sin\lambda & \cos\varphi \\ -\sin\lambda & \cos\lambda & 0 \\ \cos\varphi\cos\lambda & \cos\varphi\sin\lambda & \sin\varphi \end{bmatrix}$$ (25)

225 The φ and λ are rover geodetic coordinates.

226   The covariance matrix of mean values computed from the whole observational day is:

227 $$\mathbf{C_{NEU_{mean}}} = \mathbf{D}\mathbf{C_{NEU_{set}}}\mathbf{D^T} = \frac{1}{n^2}\sum_{i=1}^{n}\mathbf{C_{NEU_{ep_i}}}$$ (26)

228 where $\mathbf{C_{NEU_{set}}}$ is a block matrix which contains on the diagonal the covariance matrixes in the NEU setup from all measured

229 epochs (n) and $\mathbf{D}$ is treated as a transition matrix from the NEU to their mean values:

$$
230 \quad \mathbf{D} = \begin{bmatrix} \dfrac{1}{n} & 0 & 0 & \vdots & \dfrac{1}{n} & 0 & 0 & \cdots & \vdots & \dfrac{1}{n} & 0 & 0 \\ 0 & \dfrac{1}{n} & 0 & \vdots & 0 & \dfrac{1}{n} & 0 & \cdots & \vdots & 0 & \dfrac{1}{n} & 0 \\ 0 & 0 & \dfrac{1}{n} & \vdots & 0 & 0 & \dfrac{1}{n} & \cdots & \vdots & 0 & 0 & \dfrac{1}{n} \end{bmatrix} \qquad (27)
$$

3 Numerical experiment and discussion

231

232   In this section, the explanation of the research concept will be done. Next, the appropriate numerical experiment in
233   view of graphics and numeric settings. The parallel discussion about obtained results for appropriate interpretation will be
234   made.

3.1 Research concept

235

236   The numerical experiment is based on real single frequency code pseudorange observations from Global Positioning
237   System (GPS). Namely, C1C code data on the L1 carrier frequency (1575.42 MHz). Continuing, three different EURE
238   Permanent GNSS Network stations have been chosen in Scandinavia. Two stations in Sweden – Visby (VIS) and Skellefteå
239   (SKE), one in Norway – Vardø (VARS). The observational files and initial coordinates of receivers was gained from the
240   BKG (Bundesamt für Kartographie und Geodäsie) GNSS Data Center. The parameters of satellite orbits (SP3 file) and
241   atmospheric data were obtained by means of CDDIS (Crustal Dynamics Data Information System) - in fact, IONEX
242   (IONosphere map EXchange format) only in view of atmospheric data, as a source of IGS TEC map. The coordinates of
243   points were treated as the true coordinates in the practical part of the experiment. The reference coordinates are presented in
244   the table:

245   **Table 1.** Actual coordinates of points

Points	X	Y	Z
VIS600SWE	3246466.556	1077901.829	5365279.606
SKE800SWE	2534032.877	9751679.370	5752078.718
VARS00NOR	1844607.623	1109719.107	5983936.007

246

247   In the models, the actual coordinates have been converted to the antenna phase center to make a comparative analysis with
248   the SPP results, where measurements were executed to the antenna phase center.
249   Three different localizations allow checking how the modified SPP model works on different geodetic latitude because
250   of ionosphere activity changes, so its quality in the GPS code domain can be widely stated.
251   The research concept focuses on measurement on two different days in the cited locations. Therefore, three stations of
252   the EUREF Permanent GNSS Network were employed for comparative analysis based on data from two parallel days.

  Table 2. Experiment concept

Points	Days	SPP approaches
VIS	15/06/2019 15/08/2019	SPP with Klobuchar algorithm (SPPwithKM) Modified SPP with Vertical Total Electron Content estimation (MSPPwithdVTEC) SPP with IGS TEC map (SPPwithITM)
SKE	15/06/2019 15/08/2019	SPP with Klobuchar algorithm (SPPwithKM) Modified SPP with Vertical Total Electron Content estimation (MSPPwithdVTEC) SPP with IGS TEC map (SPPwithITM)
VARS	15/06/2019 15/08/2019	SPP with Klobuchar algorithm (SPPwithKM) Modified SPP with Vertical Total Electron Content estimation (MSPPwithdVTEC) SPP with IGS TEC map (SPPwithITM)

To execute the numerical experiment of the research , the MATLAB environment from The MathWorks was used. The "PostCalc" software developed by Dawid Kwaśniak was utilized as the base MATLAB program. Next, the complementary changes were done by the authors of manuscript due to numerical experiment requirement..

3.2 Discussion of the experiment results

The Figures 1-3 present the distribution of *dist* values during the observational day (*Results of the positioning models*) and their average value *DIST* with appropriate mean errors in the middle (*Average results of the positioning models*). In turn, the bottom parts show the error reduction of the models (*Differences of the positioning models*). The upper part of Figure 1(**a**) demonstrates the solutions for Visby station on 15 June, 2019. The *dist* results are significantly improved for **MSPPwithdVTEC** referring to the **SPPwithKM** what is confirmed by the average value of *DIST* equalled to 4.886 m. There is not a major difference of *DIST* between **MSPPwithdVTEC** and **SPPwithITM** (0.033 m). Therefore, the mean error of *DIST* (0.072 m) affirms the precision of the modified solution. Studying the bottom division of Figure 1(**a**), **SPPwithKM** was assumed as a reference one (100%) in the calculation of the percent values of error reduction based on *DIST*. The results are satisfying because of error reduction on the level of 22.97% in the **MSPPwithdVTEC** case and the close discrepancy with the error reduction of the **SPPwithITM** (0.53%). The second day using Visby station is 15 August, 2019. In the middle of Figure 1(**b**), *DIST* is beneficial for the **MSPPwithdVTEC** (4.912 m) compared to the reference model which leads to defining the tendency of improved accuracy in the SPP. Again, the difference in the average solutions of *DIST* between **MSPPwithdVTEC** and **SPPwithITM** is insignificant (0.055 m) according to code observations accuracy level. Thus, the accuracy of the estimation method is comparable with the IGS TEC map. Focusing on the average explanation of the *DIST* mean errors among the **MSPPwithdVTEC** (0.067 m) and the **SPPwithITM** (0.074 m), these approaches do not distinctly vary, which indicates that the proposed SPP model works well. In the bottom of Figure 1(**b**), the error reduction of **MSPPwithdVTEC** is 20.90% and is at a similar level with **SPPwithITM** (21.79%). The **SPPwithKM** proved to be the lowest accuracy method. Probably, the ionospheric corrections obtained by the coefficients from the navigation message cannot reflect the changes that take place in the ionosphere with the higher temporal accuracy. Briefly, in the first studied point, the **MSPPwithdVTEC** can be judged as the precise SPP model.
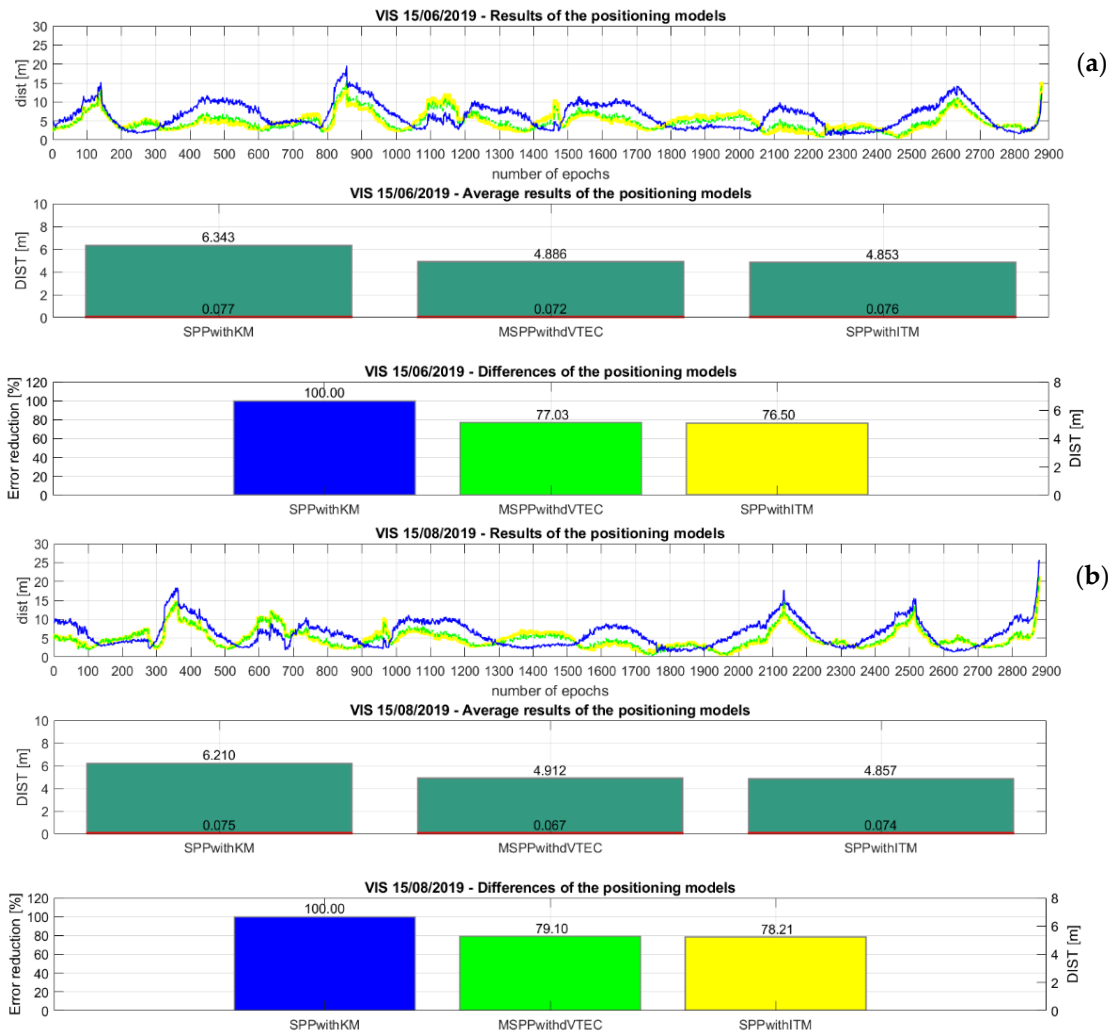
Figure 1. Set of the results of the positioning models: (**a**) VIS 15/06/2019 (**b**) VIS 15/08/2019

Following the experiment report, the next examined subject is SKE 15/06/2019. Looking at Figure 2(**a**), the top part presents the *dist* distribution of the **MSPPwithdVTEC** solutions close to the **SPPwithITM**. The average description of *DIST* validates this declaration, where the difference between these two approaches is 0.017 m, in favor of the **MSPPwithdVTEC**. In turn, according to the base model, the **MSPPwithdVTEC** delivers solutions with highly-increased accuracy, which is the most important. Despite such accuracy, the *DIST* precision of **MSPPwithdVTEC** (0.080 m) is improved and is at a similar level as **SPPwithITM** (0.093 m), which confirms the consistency of the methods. Explaining the bottom part of Figure 2(**a**), the error reduction of the **MSPPwithdVTEC** is at the beneficial level of 22.55%, which is again close to the reduction obtained by **SPPwithITM** (22.30%). Therefore, this method can be evaluated as the approach of a similar class compared to the case with IGS TEC map. The second day of tests is 15 August 2019. Based on *dist* in the top of Figure 2(**b**), it is noticeable that the **MSPPwithdVTEC** results are at related relatively similar level as **SPPwithITM.**

Looking in the middle part of Figure 2(**b**), the increased accuracy in **MSPPwithdVTEC** is verified by the *DIST* solution equal to 5.354 m, referring to the initial **SPPwithKM**. The mean error of *DIST* gives an acceptable value using **MSPPwithdVTEC** by comparable magnitude with the other models. Considering the bottom part of Figure 2(**b**), the error reduction amounts to 21.30% whereas the approach with the IGS TEC map achieves an equivalent value of 21.07%. In sum, the **MSPPwithdVTEC** can be assessed on the next EUREF's location as the valuable SPP approach by use of the new method of the ionospheric refraction estimation, without the need for external products, e.g. atmospheric factors or GIMs.
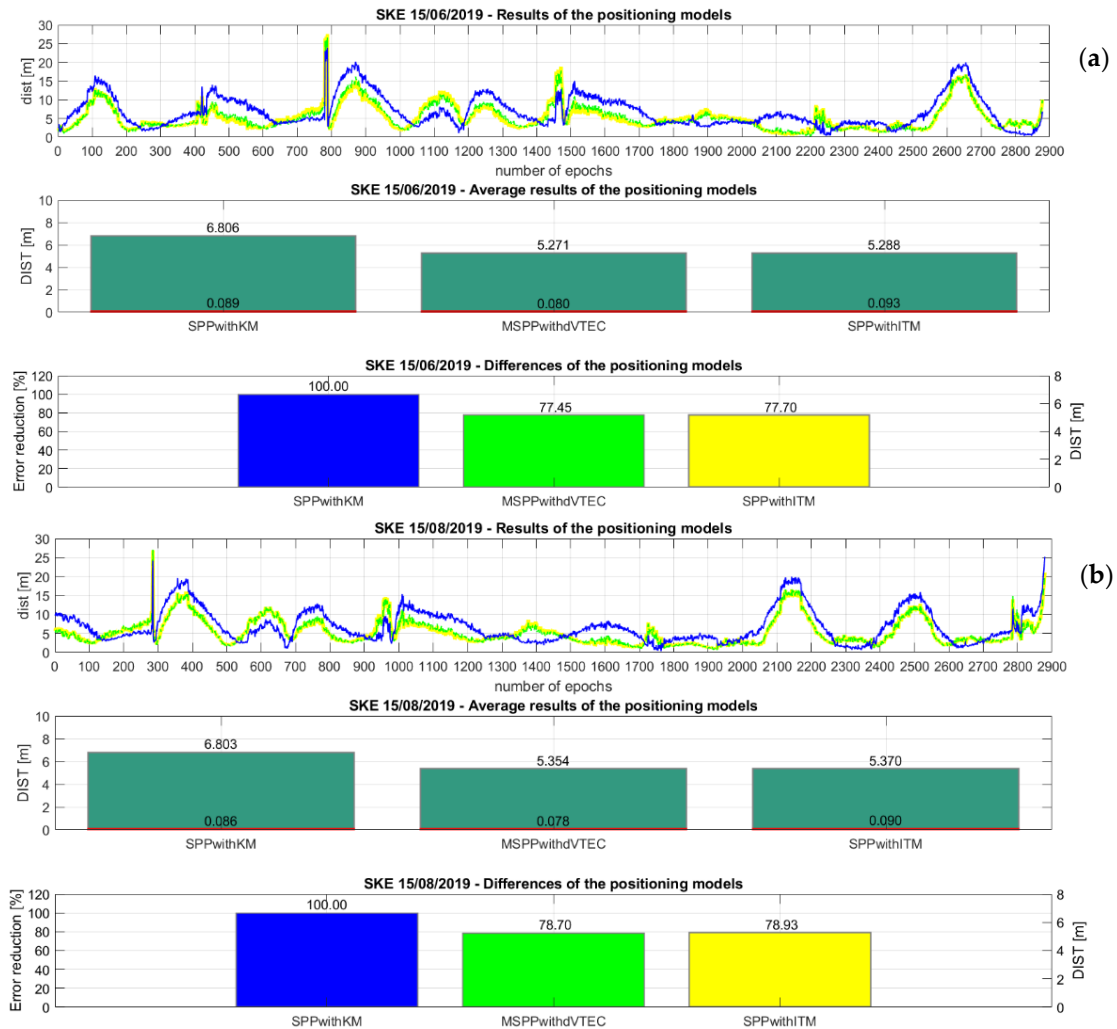
Figure 2. Set of the results of the positioning models: (**a**) SKE 15/06/2019 (**b**) SKE 15/08/2019

The last studied point is VARS00NOR. The first examined day is 15 June 2019. The middle part of Figure 3(**a**) demonstrates that the *DIST* difference of the two approaches: **SPPwithITM** and **MSPPwithdVTEC** is 0.052 m, therefore the improved accuracy is at a similar level, referring to **SPPwithKM** average observations. The precision of *DIST* confirms

the reliability of the **MSPPwithdVTEC**, where the mean error is equal to 0.087 m with an insignificant discrepancy (0.008 m) compared to the **SPPwithITM**. The bottom part of Figure 3(**a**) shows a decrease in the percent value of the error. The error reduction of the **MSPPwithdVTEC** is at the level of 16.69%, thus the improvement of accuracy is verified. Again, the difference of error reduction among **MSPPwithdVTEC** and **SPPwithITM** is on the parallel level (0.73%) which confirms the method credibility. The second tested day, and therefore the last one, is 15 August 2019. The *DIST* elaboration in Figure 3(**b**) presents the low differences between the two principal approaches on the level of 0.028 m. Studying the bottom division of Figure 3(**b**), the **MSPPwithdVTEC** achieves a positive level of error reduction of 14.91%, relating to the **SPPwithKM**. In addition, the top parts of Figure 3 (**a**) and (**b**) present the distribution of **MSPPwithdVTEC** *dist* results as close in value to the **SPPwithITM** with increased accuracy to **SPPwithKM**. This finding is also valid to other examined cases. Thus, the proposed model can be identified as stable and accurate. The error reduction is at a satisfactory level.
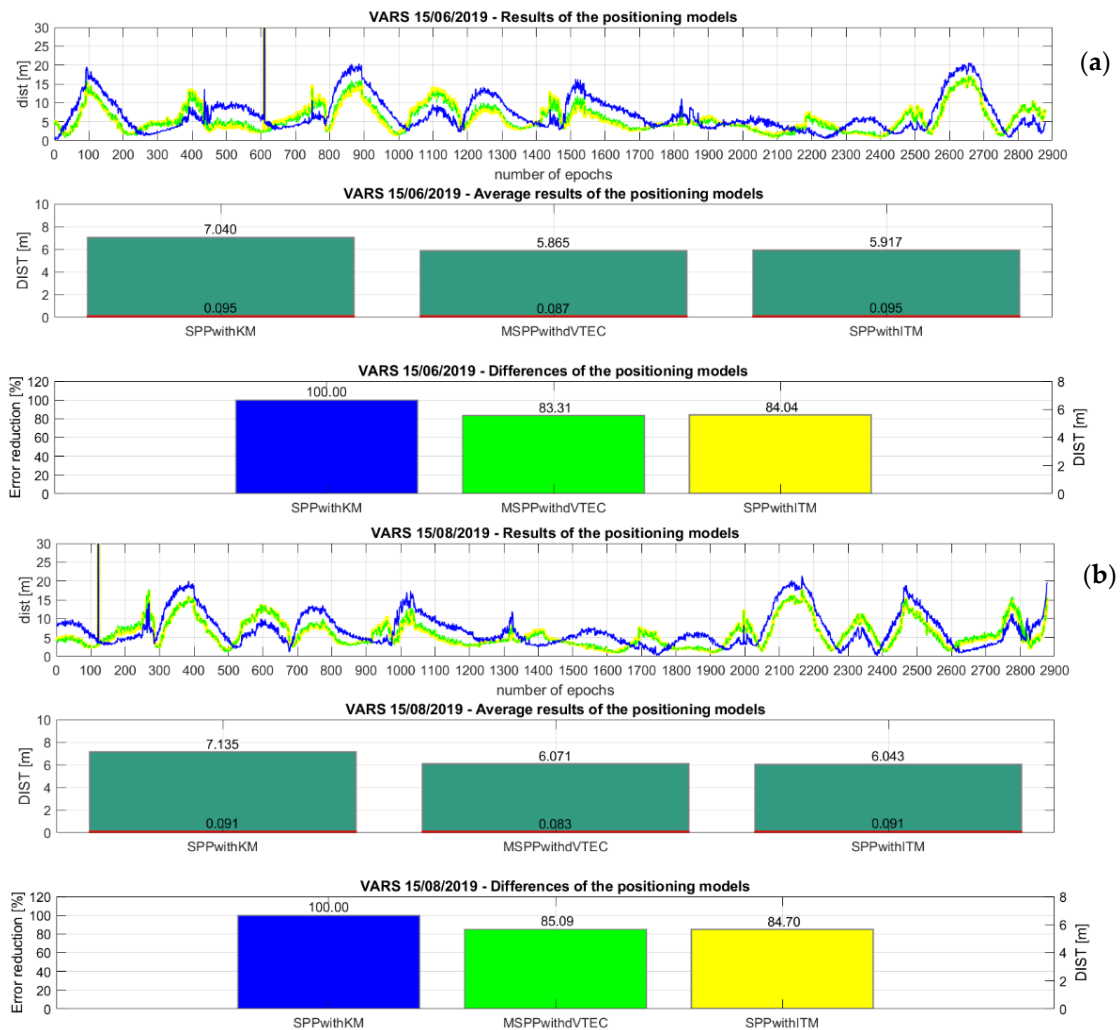
Figure 3. Set of the results of the positioning models: (**a**) VARS 15/06/2019 (**b**) VARS 15/08/2019

368   Focusing on the mean errors of the final solution in the NEU system, we will consider the average precision of the

369 differences of the components ΔN, ΔE, and ΔU, referring to the daily result. The difference means the discrepancy between

370 the actual station's coordinates and the received position from the SPP methods. For this purpose, the Eq. (28) was used to

371 determine the mean values of ΔN, ΔE and ΔU errors which are summarized in the table below:

372 **Table 3.** Average errors of the difference in the positions using the NEU system

SPP approaches	$m_{\Delta N}$	$m_{\Delta E}$	$m_{\Delta U}$	Stations and Days
SPPwithKM	0.06	0.04	0.10	
MSPPwithdVTEC	**0.05**	**0.04**	**0.09**	VIS 15/06/2019
SPPwithITM	0.06	0.04	0.09	
SPPwithKM	0.06	0.04	0.09	
MSPPwithdVTEC	**0.06**	**0.03**	**0.08**	VIS 15/08/2019
SPPwithITM	0.06	0.04	0.09	
SPPwithKM	0.05	0.03	0.11	
MSPPwithdVTEC	**0.04**	**0.03**	**0.10**	SKE 15/06/2019
SPPwithITM	0.05	0.03	0.11	
SPPwithKM	0.05	0.03	0.11	
MSPPwithdVTEC	**0.04**	**0.03**	**0.10**	SKE 15/08/2019
SPPwithITM	0.05	0.03	0.11	
SPPwithKM	0.04	0.03	0.11	
MSPPwithdVTEC	**0.04**	**0.03**	**0.10**	VARS 15/06/2019
SPPwithITM	0.04	0.03	0.11	
SPPwithKM	0.04	0.03	0.11	
MSPPwithdVTEC	**0.04**	**0.03**	**0.10**	VARS 15/08/2019
SPPwithITM	0.04	0.03	0.11	

373

374   The error quantities of the difference in the positions were achieved for **MSPPwithdVTEC** and **SPPwithITM** on a

375 close level**.** Separating the horizontal and the vertical components of the position, the **MSPPwithdVTEC** is characterized by

376 comparable precision to **SPPwithKM** in the North and East direction, therefore, the additional estimated parameter in the

377 code equation does not change the SPP model enough to reduce its quality. The case is repeated in the context of the vertical

378 component U. The **MSPPwithdVTEC** is profitable and achieves the similar values of the mean errors to **SPPwithITM**. In

379 general, the values are close to each other and the differences are not as clear in the context of the code data use. Therefore,

380 the quantities of average errors demonstrate that **MSPPwithdVTEC** is the approach of the closest precision to the

381 **SPPwithITM**, specified as a high-quality product, which is the most important from the authors' point of view.

382 **4 Conclusions and future perspectives**

383   The main idea of this paper was to introduce the new method to estimate the ionospheric delay in the SPP without using

384 the external data. Moreover, in the case of comparative analysis, two common approaches in SPP was employed: SPP with

385 Klobuchar algorithm and SPP with IGS TEC map. The first one was treated as a reference one. The SPP model with IGS

TEC map was utilized to authenticate the proposed model in view of IGS TEC map use - defined as a high-quality product. The explanation of mathematical models and appropriate accuracy analysis criteria was done. Next, the numerical experiment using real code data from three different GNSS stations with discussion to interpret the obtained results. Referring to achieved solutions, the proposed approach can be defined as a simple and independent way to improve SPP. Moreover, the **MSPPwithdVTEC** can be employed in the procedure of determination the approximate position for the need of the single-epoch precise positioning.

Based on the mean distance of the solution from the true position, the **MSPPwithdVTEC** achieved improved GPS position in comparison to the basic **SPPwithKM** in each tested station. Moreover, the **MSPPwithdVTEC** acquires a similar level of error reduction to the **SPPwithITM** what is the most satisfying in view of method authentication.

Finally, the results of the **MSPPwithdVTEC** confirm the potential use of the mathematical model in the SPP. The strategy should be developed in the future through the verification of model stability in the other stations since ionosphere changes are highly dependent on localization. Therefore, the proposed method of SPP can be recognized as a good forecast to become independent of external products delivering information about the ionospheric delay.

Competing interests. The authors declare that they have no conflict of interest.

Founding. This research is supported by grant No. 2018/31/B/ST10/00262 from the Polish National Science Centre.

References

Abdelazeem, M., Çelik, R., and El-Rabbany, A.: An Enhanced Real-Time Regional Ionospheric Model Using IGS Real-Time Service (IGS-RTS) Products, The Journal of Navigation, 69, 521-530, https://doi.org/10.1017/S0373463315000740, 2016.

Allain, D.J. and Mitchell, C.N.: Ionospheric delay corrections for single-frequency GPS receivers over Europe using tomographic mapping, GPS Solutions, 13, 141-151, https://doi.org/10.1007/s10291-008-0107-y, 2009.

Awange, J.L.: Environmental Monitoring using GNSS, 1st ed., Springer-Verlag, Berlin/Heidelberg, Germany, 2012.

Bakuła, M.: Precise Method of Ambiguity Initialization for Short Baselines with L1-L5 or E5-E5a GPS/GALILEO Data, Sensors, 18, 4318, https://doi.org/10.3390/s20154318, 2020.

Bosy, J.: Scientific journals of the Agricultural Academy in Wrocław CCXXXIV (no. 522): Precise Processing of satellite GPS observations in local networks located in mountain areas, 1st ed., Publishing house of the Agricultural Academy, Wrocław, Poland, 2005.

Chen, K. and Gao, Y.: Real-Time Precise Point Positioning Using Single-Frequency Data, in: Proceedings of the 18th International Technical Meeting of the Satellite Division of The Institute of Navigation, Long Beach, USA, September 2005.

Ciećko, A. and Grunwald, G.: Klobuchar, NeQuick G, and EGNOS Ionospheric Models for GPS/EGNOS Single-Frequency Positioning under 6-12 September 2017 Space Weather Events, Applied Sciences, 10, 1553, https://doi.org/10.3390/app10051553, 2020.

Ciraolo, L.: Ionospheric Total Electron Content (TEC) from the Global Positioning System, in: Proceedings of the XXVIIIth URSI General Assembly, New Delhi, India, October 2005.

Cooper, C., Mitchell, C.N., Wright, C.J., Jackson, D.R., and Witvliet, B.A.: Measurement of Ionospheric Total Electron Content Using Single-Frequency Geostationary Satellite Observations, Radio Science, 54, 10-19, https://doi.org/10.1029/2018RS006575, 2019.

de Camargo, P.O., Monico, J.F.G., and Ferreira, L.D.D.: Application of ionospheric corrections in the equatorial region for L1 GPS users, Earth Planet Space, 52, 1083-1089, https://doi.org/10.1186/BF03352335, 2000.

El-Rabbany, A.: Introduction to GPS: The Global Positioning System, 1st ed., Artech House Mobile Communications Series, Norwood, USA, 2002.

Georgiadiou, P.Y.: Modeling the ionosphere for an active control network of GPS stations, LGR - series: publications of the Delft Geodetic Computing Centre, 7, 1994.

Golubkov, G.V., Manzhelii, M.I. and Eppelbaum, L.V.: Quantum Theory of Disturbance and Delay of GPS Signals in D and E Atmospheric Layers: An Introduction, Positioning, 9, 13-22, https://doi.org/10.4236/pos.2018.92002, 2018.

Golubkov, G.V., Manzhelii, M.I. and Eppelbaum, L.V.: Quantum Nature of Distortion and Delay of Satellite Signals II, Positioning, 9, 47-72, https://doi.org/10.4236/pos.2018.93004, 2018.

Hofmann-Wellenhof, B., Lichtenegger, H., and Wasle, E.: GNSS – Global Navigation Satellite Systems, 1st ed., Springer-Verlag, Wien, Austria, 2008.

Hopfield, H.S.: Two-quartic tropospheric refractivity profile for correcting satellite data, Oceans and Atmospheres, 74, 4487-4499, https://doi.org/10.1029/JC074i018p04487, 1969.

Klobuchar, J.A.: Ionospheric Time-Delay Algorithm for Single-Frequency GPS Users, IEEE Transactions on Aerospace and Electronic Systems, AES-23, 325-331, https://doi.org/10.1109/TAES.1987.310829, 1987.

Krypiak-Gregorczyk, A., Wielgosz, P., and Borkowski, A.: Ionosphere Model for European Region Based on Multi-GNSS Data and TPS Interpolation, Remote Sensing, 9, 1221, https://doi.org/10.3390/rs9121221, 2017.

Krypiak-Gregorczyk, A. and Wielgosz, P.: Carrier phase bias estimation of geometry-free linear combination of GNSS signals for ionospheric TEC modeling, GPS Solutions, 22, 45 (2018), https://doi.org/10.1007/s10291-018-0711-4, 2018.

Kuverova, V.V., Adamson, S.O., Berlin, A.A., Bychkov, V.L., Dmitriev, A.V., Dyakov, Y.A., Eppelbaum, L.V., Golubkov, G.V., Lushnikov, A.A., Manzhelii, M.I., Morozov, A.N., Nabiev, S.S., Suvorova, A.V., Golubkov, M.G.: Chemical physics of D and E layers of the ionosphere, Ad. in Space Research, 63, 1876-1886, https://doi.org/10.1016/j.asr.2019.05.041, 2019.

Leick, A., Rapoport, L., and Tatarnikov, D.: GPS Satellite Surveying, 4th ed., John Wiley & Sons, Hoboken, USA, 2015.

Prol, F.S., Camargo, P.O., and Muella, M.T.A.H.: Comparative study of methods for calculating ionospheric points and describing the GNSS signal path, Boletim de Ciências Geodésicas, 23, 669-683, http://dx.doi.org/10.1590/s1982-21702017000400044, 2017.

Rui, T., Qin, Z., Guanwen, H., and Hong, Z.: On ionosphere-delay processing methods for single-frequency precise-point positioning, Geodesy and Geodynamics, 2, 71-76, https://doi.org/10.3724/SP.J.1246.2011.00071, 2011.

Setti Júnior, P.T., Alves, D.B.M., and Silva, C.M.: Klobuchar and Nequick G ionospheric models comparison for multi-GNSS single-frequency code point positioning in the Brazilian region, Boletim de Ciências Geodésicas, 25, e2019016, https://doi.org/10.1590/s1982-21702019000300016, 2019.

Stępniak, K.: Analysis on the influence of advanced GNSS signal tropospheric delay modeling methods on estimated coordinates of ASG-EUPOS stations, Ph. D. thesis, University of Warmia and Mazury, Olsztyn, 2016.

Strang, G. and Borre, K.: Linear Algebra, Geodesy, and GPS, 1st ed., Wellesley-Cambridge Press, Wellesley, USA, 2008.

Schüler, T.: On Ground-Based GPS Tropospheric Delay Estimation, Ph.D. thesis, Bundeswehr University, München, 2001.

Teunissen, P.J.G. and Kleusberg, A.: GPS for Geodesy, 2nd ed., Springer-Verlag, Berlin/Heidelberg, Germany, 1998.

US Army Corps of Engineers: NAVSTAR Global Positioning System Surveying, 2nd ed., Department of the Army US Army Corps of Engineers, Washington, USA, 2003.

463   Xu, G.: GPS Theory, Algorithms and Applications, 2nd ed., Springer-Verlag, Berlin/Heidelberg, Germany, 2007.

464   Xu, G. and Xu, Y.: GPS Theory, Algorithms and Applications, 3rd ed., Springer-Verlag, Berlin/Heidelberg, Germany, 2016.

465   Zhang, L., Yao, Y., Peng, W., Shan, L., He, Y., and Kong, J.: Real-Time Global Ionospheric Map and Its Application in
466   Single-Frequency Positioning, Sensors, 19, 1138, https://doi.org/10.3390/s19051138, 2019.